universe

IMPACT FACTOR 2.6

CITESCORE 5.2

Article

Bethe–Heitler Cascades and Hard Gamma-Ray Spectra in Flaring TeV Blazars: 1ES 0414009 and 1ES 1959650

Samuel Victor Bernardo da Silva, Luiz Augusto Stuani Pereira and Rita de Cássia Dos Anjos

Special Issue
10th Anniversary of *Universe:* Galaxies and Their Black Holes

Edited by
Dr. Paola Marziani and Prof. Dr. Mauro D'Onofrio

MDPI

https://doi.org/10.3390/universe11060177 *universe*

MDPI

Article

Bethe–Heitler Cascades and Hard Gamma-Ray Spectra in Flaring TeV Blazars: 1ES 0414+009 and 1ES 1959+650

Samuel Victor Bernardo da Silva [1,*,†], **Luiz Augusto Stuani Pereira** [1,2,*,†] and **Rita de Cássia Dos Anjos** [3,4,5,6,7,8,*]

1 Unidade Acadêmica de Física, Universidade Federal de Campina Grande (UAF-UFCG), R. Aprígio Veloso, 882, Campina Grande 58429-900, PB, Brazil
2 Instituto de Física, Universidade de São Paulo (IFUSP), R. do Matão, 1371, São Paulo 05508-090, SP, Brazil
3 Programa de póS-Graduação em Física, Departamento de Física, Universidade Estadual de Londrina (UEL), Rodovia Celso Garcia Cid Km 380, Londrina 86057-970, PR, Brazil
4 Programa de Pós-Graduação em Física e Astronomia, Universidade Tecnológica Federal do Paraná (UTFPR), Av. Sete de Setembro, 3165, Curitiba 80230-901, PR, Brazil
5 Max-Planck-Institut für Kernphysik, Saupfercheckweg 1, 69117 Heidelberg, Germany
6 Departamento de Engenharias e Exatas, Universidade Federal do Paraná (UFPR), Rua Pioneiro, Palotina 85950-000, PR, Brazil
7 Programa de Pós-Graduação em Física Aplicada, Universidade Federal da Integração Latino-Americana, Av. Tarquínio Joslin dos Santos, 1000, Foz do Iguaçu 85867-670, PR, Brazil
8 Departamento de Física, Universidade Federal do Espírito Santo, Núcleo de Astrofísica e Cosmologia (Cosmo-Ufes), Av. Fernando Ferrari, 514, Vitória 29075-910, ES, Brazil
* Correspondence: samuel.bernardo@estudante.ufcg.edu.br (S.V.B.d.S.); luizstuani@uaf.ufcg.edu.br (L.A.S.P.); ritacassia@ufpr.br (R.d.C.D.A.)
† These authors contributed equally to this work.

Abstract: In this work, we present updated models of the spectral energy distributions (SEDs) for two high-frequency-peaked BL Lac objects (HBLs), that is, 1ES 0414+009 and 1ES 1959+650. The hard gamma-ray spectra observed during their flaring states suggest the presence of an additional emission component beyond the standard synchrotron self-Compton (SSC) scenario. We explore the possibility that this hard gamma-ray emission arises from inverse Compton (IC) scattering by Bethe–Heitler pairs produced along the line of sight, pointing to a more complex high-energy emission mechanism in these sources.

Keywords: high-synchrotron peaked BL Lacs; spectral energy distribution; Bethe–Heitler pair production

check for updates

Academic Editors: Mauro D'Onofrio and Paola Marziani

Received: 29 April 2025
Revised: 28 May 2025
Accepted: 29 May 2025
Published: 31 May 2025

Citation: Bernardo da Silva, S.V.; Stuani Pereira, L.A.; Dos Anjos, R.d.C. Bethe–Heitler Cascades and Hard Gamma-Ray Spectra in Flaring TeV Blazars: 1ES 0414+009 and 1ES 1959+650. *Universe* **2025**, *11*, 177. https://doi.org/10.3390/universe11060177

1. Introduction

Active galactic nuclei (AGN) constitute a prominent population of energetic extragalactic sources, with blazars representing an extreme subclass of radio-loud AGN. Blazars, a subclass of jetted AGN that includes flat-spectrum radio quasars (FSRQs) and BL Lac objects (BLOs), exhibit non-thermal continuum emission originating from relativistic jets aligned close to our line of sight [1]. Moreover, they are characterized by distinctive characteristics such as rapid variability, high luminosity, and strong polarization [2–6]. FSRQs are distinguished by their strong, broad emission lines, whereas BLOs exhibit weak or nearly absent emission lines [7]. Their multiwavelength spectral energy distributions (SEDs) typically feature a characteristic double-hump structure [3,4,8–11]. The low-energy hump, spanning from the radio to the X-ray bands, is well explained by synchrotron radiation. However, the origin of the high-energy hump, which falls within the MeV-TeV energy range, remains an open question. Two theoretical models describe the high-energy photon emission in blazars: the leptonic model and the hadronic model. In the leptonic model scenarios, the high-energy component may result from inverse Compton (IC) scattering of relativistic electrons, either on synchrotron photons (Synchrotron Self-Compton, SSC [12,13]) or on external photon fields (External Compton, EC [4,14,15]), such as the broad-line region (BLR), accretion disk, or the external torus. In contrast, the hadronic model suggests that high-energy gamma-rays are generated either through proton synchrotron radiation in sufficiently strong magnetic fields [16–18] or via meson and lepton production in cascades triggered by proton-proton or proton-photon interactions [19–22].

The position of the first peak in SEDs, ν_p^S (synchrotron peak frequency), classifies the sources as low-frequency peaked BL Lacs (LBLs; e.g., $\nu_p^S < 10^{14}$ Hz), intermediate-frequency peaked BL Lacs (IBLs; e.g., 10^{14} Hz $< \nu_p^S < 10^{15}$ Hz), and high-frequency peaked BL Lacs (HBLs; e.g., $\nu_p^S > 10^{15}$ Hz) [8]. Several studies [12,23,24] have shown that the SEDs of BL Lac objects, particularly HBLs, are well described by a pure SSC model. The formation of relativistic jets in AGN remains an open question, with various models proposed to explain their origin. Two of the most well-established theories are the Blandford-Znajek mechanism [25], in which the jet derives energy from the black hole's rotation, and the Blandford-Payne mechanism [26], where the jet primarily extracts rotational energy from the accretion disk. In both scenarios, magnetic fields play a crucial role in channeling energy from the black hole or disk into the jet [27]. Initially, the jet's energy is primarily carried by Poynting flux, which progressively converts into the kinetic energy of the plasma as the flow accelerates [28]. Theoretical studies on energy dissipation suggest that, in this scenario, the emitting electrons and the electromagnetic field may share an equal distribution of energy [29]. Understanding the strength of the magnetic field within the jet is essential for unraveling its formation and energy distribution. By analyzing the frequency-dependent position of the optically thick jet core [30], Zamaninasab et al. (2014) [31] found that the jet's magnetic flux on parsec scales correlates with the power of the corresponding accretion current, aligning with predictions from magnetohydrodynamics. Another reliable approach for estimating the magnetic field in the innermost emission region of the jet is through modeling the SEDs of blazars [3,32–34].

Comparing multiwavelength emission from blazars with numerical models that simulate radiative emission and transfer under specific assumptions about particle content and emission region characteristics is a key method for investigating the source's microphysics and physical parameters. Data from the very high-energy (VHE) segment of the SED is essential for constraining model parameters of high-frequency peaked BL Lac objects, which emit a significant portion of their radiation in this energy range. Additionally, VHE observations are valuable for softer sources, as they probe the extreme limits of particle acceleration and are particularly sensitive to photon-photon absorption within internal or external radiation fields [35]. An essential element for understanding the high-energy gamma-ray emission is the Bethe-Heitler pair production (also called the proton-photon ($p\gamma$) pair production process), which occurs when relativistic protons interact with soft photons (ambient synchrotron or external photons), leading to the production of electron-positron pairs [36,37]. The generated electron-positron pairs then undergo synchrotron and IC processes, contributing to the broadband gamma-ray emission observed from blazars. It is worth mentioning that this process is typically subdominant compared to proton synchrotron or pion decay (which predict correlated neutrino and gamma-ray emissions) mechanisms in hadronic models but can still play a role in shaping the observed SED of blazars.

In this work, we investigate the SED of two blazars detected at TeV energies: 1ES 0414+009 and 1ES 1959+650. These high-energy sources provide valuable insights into particle acceleration mechanisms and emission processes. By modeling their multiwavelength emission, we aim to constrain the physical properties of their jets and explore the contribution of leptonic and hadronic processes to their observed radiation. In Section 2, we introduce our sample. In Sections 3 and 4, we present the fitting tools and the fitting process. Section 5 describes the results and provides a discussion. Finally, we present the conclusion of this work in Section 5. Throughout the paper, we assume the Hubble constant H_0 = 67.77 km s^{-1} Mpc^{-1} , the matter energy density Ω_M = 0.27, the radiation energy density Ω_r = 0, and the dimensionless cosmological constant Ω_Λ = 0.73.

2. TeV Blazars: 1ES 0414+009 and 1ES 1959+650

In this section, we are going to present a brief description of the two TeV blazars studied in this work and the set of data used in our analysis.

2.1. 1ES 0414+009

The BL Lac object 1ES 0414+009 was first detected by the HEAO 1 satellite [38] in the 0.9–13.3 keV energy range and later identified in X-ray images from the Einstein Observatory [39]. Situated at a redshift of z = 0.287 [40], it is powered by a supermassive black hole (SMBH) with a mass of approximately 2×10^9 $M_\odot$ [41]. According to the scheme proposed by [42], 1ES 0414+009 belongs to the class of HBLs, which exhibit a synchrotron-emission peak at UV/soft X-ray frequencies. In such sources, X-ray emission is primarily dominated by synchrotron radiation. In the VHE gamma-ray domain, data from the HEGRA experiment were used to establish an upper limit on the integral flux of 1ES 0414+009, corresponding to 13.5×10^{-12} cm^{-2} s^{-1} above the threshold energy of 910 GeV [43]. Costamante & Ghisellini [44] identified 1ES 0414+009 as a strong candidate for VHE emission based on its high X-ray and radio flux. Its detection became even more probable following blazar gamma-ray spectrum analyses, which suggested a low intensity of the diffuse extragalactic background light (EBL) [45].

The H.E.S.S. array of Cherenkov telescopes has detected significant VHE gamma-ray emission from 1ES 0414+009. With an average flux of ∼0.6% of the Crab Nebula flux above E > 200 GeV, this blazar is among the faintest extragalactic sources observed in the TeV range. Additionally, 1ES 0414+009 was detected by the Fermi-LAT instrument during its first 20 months of operation (2008–2010), exhibiting very faint emission in the high-energy (HE) domain as well [46]. The HE and VHE spectra of 1ES 0414+009, corrected for absorption using an EBL model close to the lower limits, exhibit a best-fit power law with an index harder than 2, classifying it as a hard-TeV BL Lac object. The overall SED is averaged over five years, though there is no strict simultaneity between Swift and H.E.S.S. observations. With this limitation, the SED properties, particularly an IC peak energy above 1–2 TeV, are challenging to explain within the framework of a pure one-zone SSC model, unless unusual parameter values are assumed [47].

The study of 1ES 0414+009 has implications beyond its characterization, extending to the broader context of AGN and their role in multi-messenger astronomy [48]. This blazar, along with others, has been proposed as a potential source of ultra-high-energy cosmic rays [49]. These investigations collectively enhance our understanding of the extreme environments surrounding supermassive black holes and their relativistic jets, contributing to advancements in high-energy astrophysics [50,51].

2.2. 1ES 1959+650

The object 1ES 1959+650 [52], with a redshift of z = 0.047, was classified as a BL Lac in 1993 using a specialized radio/optical/X-ray technique [53]. Its first detection at TeV energies was reported by the Utah Seven Telescope Array collaboration during the 1998 observational season [54], revealing an excess with a statistical significance of 3.9σ above 600 GeV after 57 h of observation. In May 2002, 1ES 1959+650 experienced a powerful

TeV outburst, observed by the VERITAS [55], HEGRA [56] collaborations. Significant flux variations were recorded, reaching levels up to three times the Crab Nebula flux [57].

As a HBL source, 1ES 1959+650 is generally faint in the *Fermi*-LAT energy range (20 MeV–300 GeV) compared to nearby LBLs and exhibits weaker variability in this band than in the X-ray and VHE ranges [58]. Notably, the 0.3–10 GeV flux did not display significant long-term flares, with the photon flux derived from two-week binned data rarely exceeding 4×10^{-8} photons $\mathrm{cm}^{-2}\,\mathrm{s}^{-1}$ [59–61]. However, the source remained mostly above this threshold between August 2015 and August 2016, during which two strong, long-term HE flares were observed [62,63].

During intense X-ray flares in 2016–2017, the source exhibited very hard X-ray spectra, with the 0.3–300 GeV photon index also remaining hard during the same periods [63]. While reproducing such hard gamma-ray spectra can be challenging for standard leptonic models, certain hadronic scenarios may offer a more natural explanation under specific conditions [64]. For example, the proton blazar model introduced by Mannheim [20] predicts X-ray spectra with photon indices in the range 1.5–1.7 and can account for uncorrelated X-ray–TeV variability, a feature reported for this source [58]. Nonetheless, leptonic models remain widely favored in the literature (e.g., [12]), and further multiwavelength studies are needed to distinguish between competing scenarios.

3. Multi-Wavelength SED Fitting of Jetted AGNs

Modeling the SEDs of jetted AGN across the electromagnetic spectrum, from radio to gamma-rays, is essential for understanding the physical mechanisms governing relativistic jets. Through multiwavelength SED fitting, we can investigate particle acceleration, energy dissipation, and radiative processes responsible for the observed emission.

3.1. SED Leptonic Modeling

We employed the JetSeT v1.3.0 software package [65–67] for leptonic SED modeling. JetSeT is an open-source C/Python framework designed to simulate radiative and particle acceleration processes in relativistic jets and galactic sources, both beamed and unbeamed. It supports various leptonic emission mechanisms, including synchrotron radiation, SSC, and external Compton (EC) scattering of photons from the accretion disk, BLR, dusty torus (DT), and the cosmic microwave background (CMB). The framework also includes $\gamma\gamma$ absorption based on established EBL models [68–70].

To ensure consistency across sources, we adopted a one-zone synchrotron+SSC scenario, where the emission originates from a spherical region of radius $R = ct_{\rm var}\delta/(1+z)$ [71], with $t_{\rm var}$ set to one day [72,73]. The region moves relativistically with a Doppler factor $\delta = [\Gamma(1-\beta\cos\theta)]^{-1}$, where Γ is the bulk Lorentz factor and θ the viewing angle. Electrons are assumed to follow a broken power-law distribution [12,23,28]:

$$N(\gamma) = N_0 \begin{cases} \gamma^{-p_1}, & \gamma_{\rm min} \leq \gamma \leq \gamma_{\rm b}, \\ \gamma_b^{p_2-p_1}\gamma^{-p_2}, & \gamma_{\rm b} < \gamma \leq \gamma_{\rm max}, \end{cases} \tag{1}$$

where $\gamma_{\rm min}$, $\gamma_{\rm b}$, and $\gamma_{\rm max}$ are the minimum, break, and maximum electron Lorentz factors, and N_0 is the normalization constant.

JetSeT employs a two-stage fitting procedure. First, a phenomenological characterization of the SED is performed using the `SEDShape` module, which applies power-law and log-parabolic fits to binned data spanning the radio to TeV range. This step provides initial constraints on the synchrotron and SSC components, helping to define parameter boundaries. Next, the `ObsConstrain` module is used to derive input parameters for the physical modeling, where we adopt the broken power-law electron distribution defined in

Equation (1). A Bayesian approach is adopted for the final model fitting, incorporating prior constraints to ensure that all parameters remain within physically meaningful bounds.

Model parameters are implemented as Astropy quantities, allowing seamless integration with other Python-based astrophysical tools. JetSeT supports both frequentist and Bayesian fitting approaches. For frequentist optimization, plugins are available for `iminuit` [74] and SciPy's bounded least squares method [75]. Bayesian inference is carried out using a Markov chain Monte Carlo (MCMC) sampler through integration with the `emcee` package [76]. In all cases, the redshift is fixed, and we assume a cold proton to relativistic electron ratio of 0.1 [77].

3.2. SED Lepto-Hadronic Modeling

To explore scenarios involving hadronic contributions, we used the AM^3 (astrophysical multi-messenger modeling) framework [78], an open-source software package designed to simulate time-dependent lepto-hadronic interactions in astrophysical sources. AM^3 computes the coupled evolution of photon, electron, positron, proton, neutron, and neutrino populations, along with intermediate products, within an isotropic magnetic field. It includes non-linear processes such as electromagnetic cascades and secondary particle feedback, providing a self-consistent description of particle interactions.

The emission region is modeled as a spherical blob of radius R' moving with bulk Lorentz factor Γ along the jet. Primary electrons and protons are injected isotropically into this region. Electrons follow a broken power-law energy distribution, while protons follow a single power-law extending up to $\gamma'_{\mathrm{p,max}}$. These high-energy protons interact with ambient photon fields following the framework of Hümmer et al. (2010) [79], producing charged and neutral pions. The decay of pions gives rise to secondary gamma-rays, neutrinos, electrons, and positrons, which in turn participate in electromagnetic cascades.

AM^3 incorporates several key processes: synchrotron emission and self-absorption, IC scattering by both electrons and protons, Bethe–Heitler pair production ($p + \gamma \rightarrow p + e^- + e^+$), photon-photon pair production and annihilation, and the evolution of secondary particles. The magnetic field B' is assumed to be randomly oriented within the blob, and its turbulence plays a significant role in shaping the resulting SED and multi-messenger signatures.

This approach allows us to assess the hadronic contribution to the SED and explore scenarios where neutrino and gamma-ray emission arise from the same physical region, providing insight into possible associations between high-energy astrophysical neutrinos and blazar flares.

4. Results and Discussions

Based on the methods presented in Sections 3.1 and 3.2, it was possible to perform the non-thermal multi-wavelength modeling of the blazars 1ES 0414+009 and 1ES 1959+650. For this, data from space and ground-based observatories, ranging from radio to VHE gamma-rays, were extracted from the Space Science Data Center (SSDC)[1] and Firmamento[2]. First, the multi-wavelength observations were fitted using the MCMC method in JetSeT, and the best-fitting parameters were then used as input for the lepto-hadronic modeling with AM^3. Tables 1 and 2 summarize the observatories employed in the modeling of the sources 1ES 0414+009 and 1ES 1959+650, respectively, together with the corresponding energy/wavelength ranges covered by the data collected at each facility.

Table 1. Observatory catalogs used in the modeling of the broadband SED of the source 1ES 0414+009, listed with their respective energy ranges and references.

Observatory/Instrument	Catalog(s)	Energy/Wavelength Range	Catalog Reference
NRAO 91-m Telescope	NORTH20CM	Radio (1.4 GHz)	[80]
VLA	NVSS, CRATES, CLASSSCAT	Radio (1.4–8.4 GHz)	[81–83]
Parkes Telescope	PMN	Radio (4.85 GHz)	[84]
Green Bank Telescope	GBE	Radio (4.85 GHz)	[85]
EXOSAT CMA	CMA	X-ray (0.05–2.0 keV)	[86]
ROSAT	RASS, RXS2CAT, WGACAT2	X-ray (0.1–2.4 keV)	[87–89]
Einstein IPC	IPC	X-ray (0.15–4.5 keV)	[39,52,90]
Swift-XRT	1SWXRT, 1SXPS	X-ray (0.3–10 keV)	[91,92]
BeppoSAX	BeppoSAX Spectra	X-ray/Gamma-ray (0.1–300 keV)	[93]
NASA/IPAC Database (Multi)	NED	Multi-wavelength (Radio to Gamma-ray)	[94]
Fermi-LAT	Fermi1FGL, FERMI2FGL, FERMI3FGL, 2FHL, FERMI 4FGL-DR3, BAND P5	Gamma-Ray (50 MeV–2 TeV)	[95–100]
ARGO-YBJ	ARGO2LAC	Gamma-ray (0.3–10 TeV)	[101]
VERITAS	VERITAS	VHE Gamma-ray (85 GeV–30 TeV)	[102]
H.E.S.S.	HESS	VHE Gamma-ray (100 GeV–100 TeV)	[47]

Table 2. Observatory catalogs used in the modeling of the broadband SED of the source 1ES 1959+650, listed with their respective energy ranges and references.

Observatory/Instrument	Catalog(s)	Energy/Wavelength Range	Catalog Reference
2MASS Survey	2MASS	Near-Infrared (1.25–2.17 µm)	[103]
WISE	WISE	Mid-Infrared (3.4–22 µm)	[104]
Planck	PCCS2143	Microwave (30–857 GHz)	[105]
GMRT	TGSS150	Radio (150 MHz)	[106]
Green Bank Telescope (GB)	GB6, GB87	Radio (4.85 GHz)	[85,107]
VLA	CRATES, NVSS, VLASSQL	Radio (1.4–8.4 GHz)	[81,82,108]
NRAO 91-m Telescope	NORTH20	Radio (1.4 GHz)	[80]
Pan-STARRS	PanSTARRS	Optical (400–1000 nm)	[109]
Gaia	GAIA	Optical (330–1050 nm)	[110]
HST, GSC	HSTGSC	Optical (300–1000 nm)	[111]
Compiled from multiple optical surveys	DEBL	Optical (350–950 nm)	[112]
Swift-UVOT	UVOT	UV/Optical (170–650 nm)	[113]
GALEX	GALEX	UV (135–280 nm)	[114]
XMM-Newton Optical Monitor	XMMOM	UV/Optical (180–600 nm)	[115]
Owens Valley + others	OUNBLZ, OUSXB	Optical (400–800 nm), X-ray (0.3–10 keV)	[116,117]
Einstein IPC	IPCSL	X-ray (0.16–3.5 keV)	[52]
ROSAT	RASS	X-ray (0.1–2.4 keV)	[88]
Swift-XRT	2SXPS, XRTSPEC	X-ray (0.3–10 keV)	[118,119]
XMM-Newton	4XMM-DR10, XMMSL2	X-ray (0.2–12 keV)	[120,121]
Swift-BAT	BAT105m	Hard X-ray (14–195 keV)	[122]
BeppoSAX	BeppoSAX	X-ray/Gamma-ray (0.1–300 keV)	[93]
Oulu Neutron Monitor	OULC	Cosmic-ray flux (secondary particles, ∼GeV range)	[123]
Fermi-LAT	3FGL, 4FGL-DR2, 3FHL, 2FHL, 2BIGB, FMonLC	Gamma-ray (50 MeV–2 TeV)	[95–99]
MAGIC	MAGIC	VHE Gamma-ray (50 GeV–50 TeV)	[124]
VERITAS	VERITAS	VHE Gamma-ray (85 GeV–30 TeV)	[59]
Whipple Telescope	WHIPPLE	VHE Gamma-ray (300 GeV–10 TeV)	[125]

4.1. SSC SED Fitting

In the fitting method, each free parameter has a specific physical boundary. We can fix specific parameters and set the fitting range of the remaining parameters to speed up the convergence of the fitting process. Given that all our samples are HBLs and we adopt the one-zone lepton model Syn+SSC, we fix the redshift and the distance of the radiation region from the central black hole, R_H - 10^{17} cm (default value for JetSeT). To prevent biased results, ensure that output parameters remain within physically meaningful ranges (based on the literature [102,126]), and improve convergence, we define fitting ranges for the radius of the emission region R, magnetic field strength B, γ_{min}, γ_b, γ_{max}, and the spectral indexes (p and p_1). The best-fitting values are described in Table 3.

Table 3. SSC model parameters for 1ES 0414+009 and 1ES 1959+650.

Symbol	Description	1ES 0414+009	1ES 1959+650
γ_{min}	Minimum electron Lorentz factor	6.35×10^1	9.60×10^2
γ_{break}	Break electron Lorentz factor	8.11×10^4	1.96×10^5
γ_{max}	Maximum electron Lorentz factor	1.70×10^6	2.40×10^6
B [G]	Magnetic field strength	3.62×10^{-1}	1.05×10^{-1}
R [cm]	Radius of the emitting region (blob)	1.02×10^{16}	3.15×10^{15}
θ_{obs} [deg]	Viewing angle	1.61	2.9
N [cm^{-3}]	Particle number density	45.11	12.47
p	Spectral index below γ_{break}	2.29	2.41
p_1	Spectral index above γ_{break}	4.45	4.37
Γ	Bulk Lorentz factor	15.02	37.25

Figure 1 shows the modeling via the SSC physical process for the 1ES 0414+009 source. The first peak in the figure represents the synchrotron emission, which occurs at lower frequencies, peaking at $\sim 10^{17}$ Hz, thus indicating that 1ES 0414+009 is a HSP BL Lac. The second peak, at $\sim 10^{25}$ Hz, represents the emission due to IC scattering. According to the residual plot at the bottom of the figure, the model fits the data well by plotting the difference between actual and predicted values, with only one discrepancy in the TeV region of the energy spectrum.

In JetSeT, jet power can be readily estimated by fitting the spectral energy distributions. The jet kinetic power is carried by electrons, magnetic fields, and cold protons [28,71,127], and is expressed as $L_i = \pi R^2 \Gamma^2 c U_i$, where U_i represents the energy density of each component (i = e, p, B). Consequently, the total jet kinetic power is given by $L_{kin} = L_e + L_B + L_p$. The derived energy densities and luminosities for the source 1ES 0414+009 are summarized in Table 4. The total radiative power is calculated as $L_{rad} \simeq L_{syn} + L_{SSC}$, where L_{syn} and L_{SSC} are the powers emitted through synchrotron and synchrotron self-Compton processes, respectively [13].

The comparison between the parameters of the SSC model for 1ES 0414+009 obtained in this work and those reported by Aliu et al. (2012) [102] reveals important similarities despite differences in the modeling approaches and data selections. Both studies find a comparable size for the emitting region, with $R \sim 10^{16-17}$ cm, consistent with a compact emission zone typical of high-frequency peaked BL Lac objects. In addition, the viewing angle ($\theta_{obs} \sim 1.61^{\circ}$) and the general SSC framework adopted for the SED modeling are similar, indicating a shared assumption of a relativistic jet closely aligned with the observer's line of sight. Both works also conclude that purely leptonic models face challenges in fully reproducing the broadband SED, particularly in explaining the hard TeV spectra, thus motivating the consideration of more complex scenarios, such as lepto-hadronic contributions. Although there are differences in specific parameter values, such as the minimum

Lorentz factor, magnetic field strength, and bulk Lorentz factor, these arise naturally from the focus of each study: Aliu et al. (2012) [102] emphasized modeling the TeV emission with extreme parameters, while our work provides a global fit to a broader, multiwavelength dataset. Overall, both studies reinforce the notion that 1ES 0414+009 exhibits characteristics requiring detailed modeling beyond the simplest SSC assumptions.

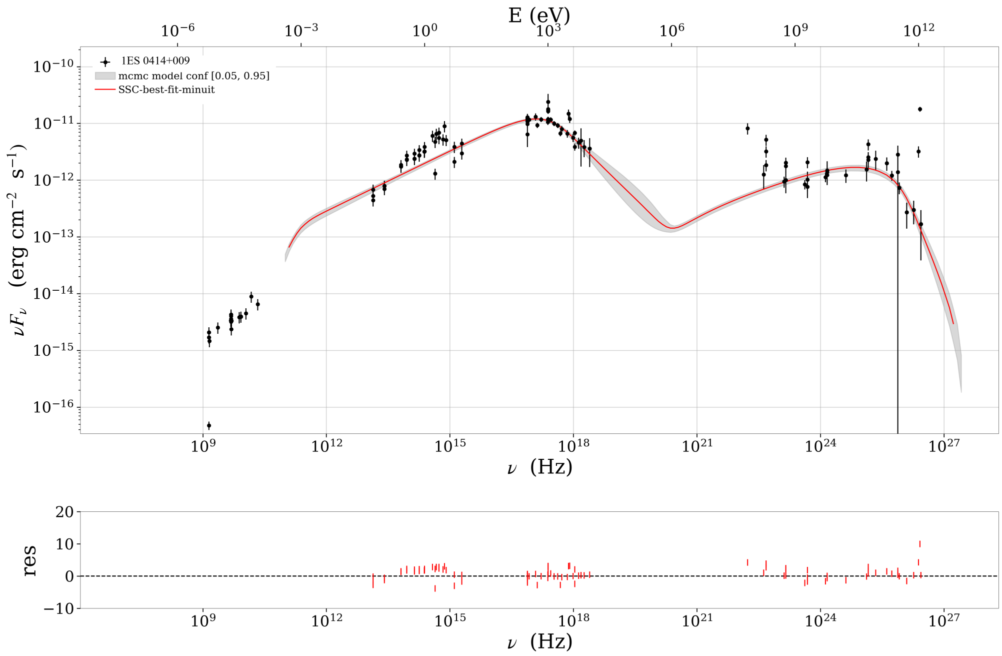

Figure 1. Broadband SED of 1ES 0414+009 modeled using a one-zone SSC model. The solid red line shows the best-fit SED, and the filled gray area represents the 1σ statistical uncertainty of the fit. Radio data points (low-energy range, $<10^{-4}$ eV) are included for completeness but are not fitted, as synchrotron self-absorption in the compact emission region renders them unconstraining within this modeling framework.

Similarly to the previous source, Figure 2 shows the modeling of 1ES 1959+650 using the SSC physical process, considering also the presence of the host galaxy component (emission peak at approximately 10^{15} Hz). As indicated by the figure, the synchrotron emission peaks at $\sim 10^{18}$ Hz, classifying the source as an extreme high-frequency peaked BL Lac (EHBL) with $\nu_{\rm sync}^{\rm peak} > 10^{16}$ Hz. The second peak, located at higher energies, is attributed to IC scattering. The best-fitting parameters are summarized in Table 3. For this source, as found for most HBLs, the kinetic powers carried by electrons and protons ($L_{\rm e}$ and $L_{\rm p}$) dominate over the magnetic contribution $L_{\rm B}$ [28].

A comparison between Tables 3 and 4 from this work and Table 5 from Tavecchio et al. (2010) [12] highlights similarities in the physical parameters derived for 1ES 1959+650. Both studies model the broadband emission using a one-zone leptonic scenario dominated by synchrotron and SSC processes, adopting similar assumptions for the jet composition and emission region structure. The magnetic field strength ($B \sim 0.1$ G) and the size of the emission region ($R \sim 3 \times 10^{15}$ cm) are consistent across the studies, suggesting comparable estimates for the energy balance within the jet. The inferred jet kinetic powers are also similar, with both analyses concluding that the power carried by particles (electrons and cold protons) largely exceeds the magnetic contribution, a common characteristic of high-frequency-peaked BL Lac objects. These similarities reinforce the model of the one-zone SSC interpretation for the quiescent state of 1ES 1959+650, as presented in both studies.

Table 4. Derived physical quantities for 1ES 0414+009 and 1ES 1959+650.

Symbol	Description	1ES 0414+009	1ES 1959+650
U_e [erg cm^{-3}]	Electron energy density	9.19×10^{-3}	3.04×10^{-2}
U_B [erg cm^{-3}]	Magnetic energy density	5.22×10^{-3}	4.37×10^{-4}
$U_{\rm sync}$ [erg cm^{-3}]	Synchrotron photon energy density	1.22×10^{-3}	3.54×10^{-4}
$L_{\rm syn}$ [erg s^{-1}]	Synchrotron radiative power	3.33×10^{42}	3.98×10^{41}
$L_{\rm SSC}$ [erg s^{-1}]	SSC radiative power	5.83×10^{41}	1.81×10^{41}
$L_{\rm rad}$ [erg s^{-1}]	Total radiated power	3.91×10^{42}	5.79×10^{41}
$L_{\rm kin}$ [erg s^{-1}]	Jet kinetic power	2.09×10^{44}	5.52×10^{43}

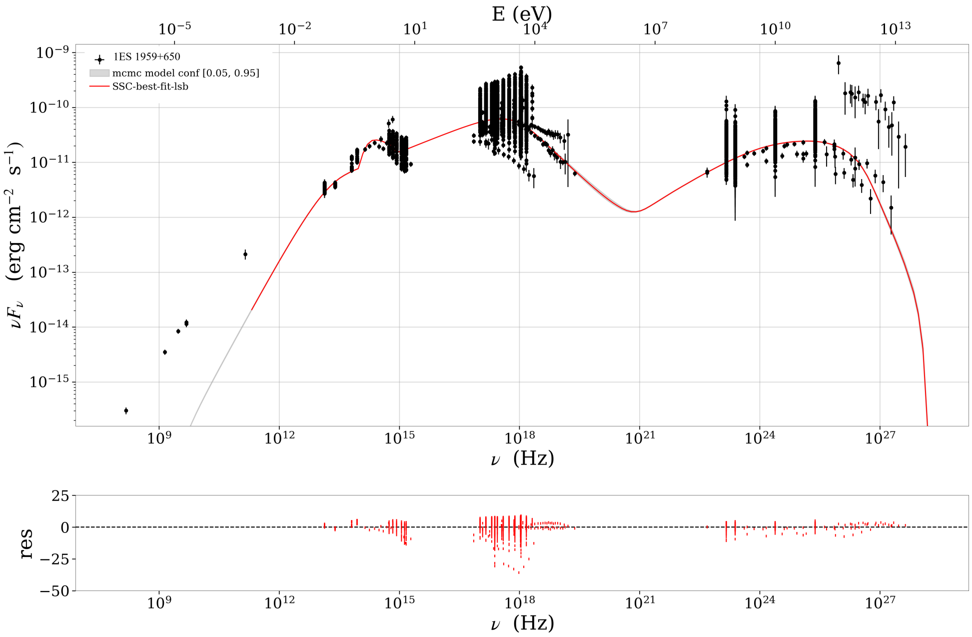

Figure 2. Broadband SED of 1ES 1959+650 modeled using a one-zone SSC model. The solid red line shows the best-fit SED, and the filled gray area represents the 1σ statistical uncertainty of the fit. Radio data points (low-energy range, <10^{-3} eV) are included for completeness but are not fitted, as synchrotron self-absorption in the compact emission region renders them unconstraining within this modeling framework.

4.2. Lepto-Hadronic SED Modeling

The lepto-hadronic SED modelling was performed using the open-source AM^3 software. The non-thermal lepton distribution in the source came from the JetSeT fitting process (section above), where the electron luminosity in the jet is $L_{\rm e} \sim 2.50 \times 10^{43}$ erg/s for 1ES 0414+009 and $L_{\rm e} \sim 3.93 \times 10^{43}$ erg/s for 1ES 1959+650. For the hadronic interaction process, the proton luminosity $L_{\rm p}$ was estimated to be less than or equal to the Eddington luminosity ($L_{\rm p} \leq L_{\rm Edd}$) [128], where $L_{\rm Edd} = 1.3 \times 10^{38}(M_{\rm BH}/M_\odot)$ erg/s. Assuming that $M_{\rm BH} \sim 2 \times 10^9$ M$_\odot$ for 1ES 0414+009 [47], $L_{\rm Edd} \sim 2.52 \times 10^{47}$ erg/s. For 1ES 1959+650 we also assumed $L_{\rm p} \leq L_{\rm Edd}$ [128], where $M_{\rm BH} \sim 3.16 \times 10^8$ M$_\odot$ [129] and the resulting Eddington luminosity is $L_{\rm Edd} \sim 3.98 \times 10^{46}$ erg/s. Although jet loading at super-Eddington rates may occur during brief episodes of flaring activity, it is unrealistic to expect such conditions to persist during extended periods of steady, quiescent emission [128]. For both sources, the injection of protons follows a simple power-law distribution with $\gamma_{\rm min} = 100$, $\gamma_{\rm max} = 10^6$ and $\alpha_{\rm p} = 1$ (spectral index).

Figure 3 and 4 display the multiwavelength SED for the blazars 1ES 0414+009 and 1ES 1959+650 along with observational data from several catalogs, including BeppoSAX, VERITAS, *Fermi*-LAT and others, covering frequencies from radio to gamma-rays. The dark blue and red lines correspond to synchrotron emission and IC scattering of primary electrons (best fitting parameters from JetSeT). The black line represents synchrotron emission and IC scattering of protons. The light blue line represents Bethe-Heitler pair production ($p\gamma \to pe^+e^-$) from 10^{-3} eV to 10^{15} eV (in the case of 1ES 0414+009) and 10^{16} eV (in the case of 1ES 1959+650). The green line refers to the synchrotron emission and IC scattering of electron-positron pair production ($\gamma\gamma \to e^+e^-$), which is observed in the energy range from 10^{-3} eV to 10^{15} eV (in the case of 1ES 0414+009) and 10^{17} eV (in the case of 1ES 1959+650). The yellow line corresponds to the multi-wavelength emission from proton-photon interaction generating charged pions ($p\gamma \to \pi^\pm \to \mu^\pm \to e^\pm$) in the range from 10^{-1} eV to 10^{15} eV (in the case of 1ES 0414+009) and 10^{17} eV (in the case of 1ES 1959+650). The purple dotted curve illustrates the gamma-ray emission resulting from the decay of neutral pions produced in proton–photon interactions ($p\gamma \to \pi^0 \to \gamma\gamma$) observed in the range from 10^{11} eV to 10^{16} eV (in the case of 1ES 0414+009) and 10^{10} eV to 10^{17} eV (in the case of 1ES 1959+650). The gamma-ray emission from the decay of neutral pions produced in proton–proton interactions ($pp \to \pi^0 \to \gamma\gamma$) is illustrated by the dark blue dashed line, which is observed in the range 10^{11} eV to 10^{15} eV (in the case of 1ES 0414+009) and 10^9 eV to 10^{17} eV (in the case of 1ES 1959+650).

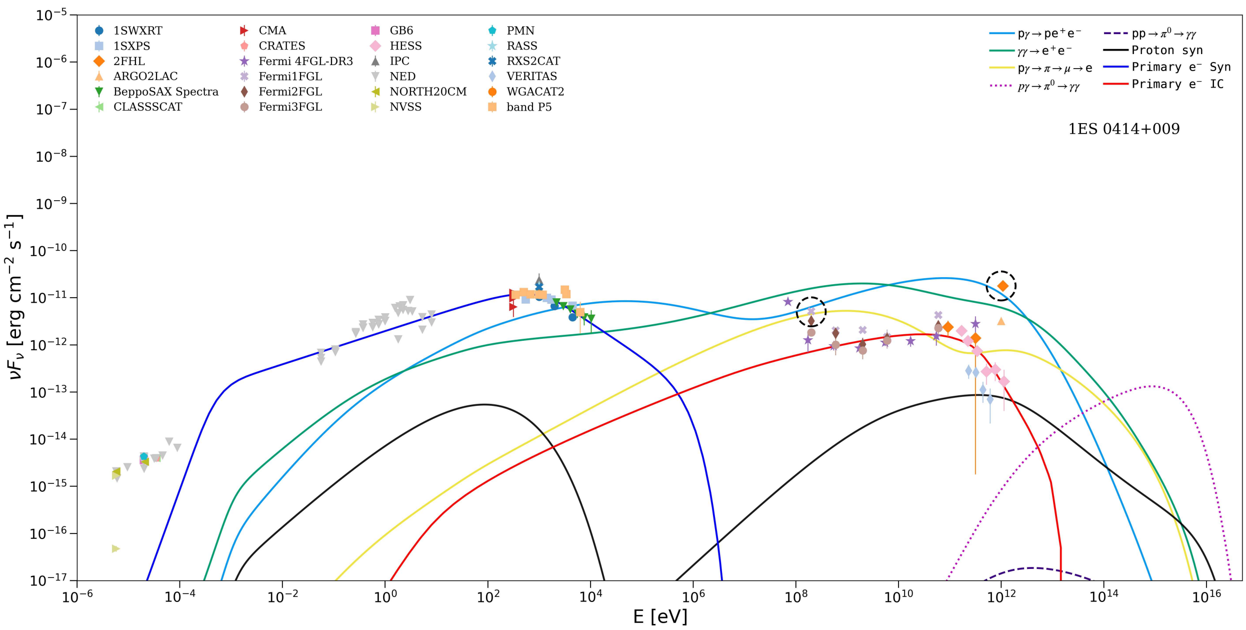

Figure 3. Lepto-hadronic SED modeling and multi-wavelength data of 1ES 0414+009 (see Table 1 for detailed observatory data used in the modeling). In comparison to the purely leptonic model, the lepto-hadronic model is characterized by the dominant contributions to the emissions of high-energy photons and neutrinos. These processes originate from the following interactions: proton–photon interactions ($p\gamma$, purple dotted curve) are observed from 10^{11} eV to 10^{17} eV. Pion production from proton–proton interactions ($pp \to \pi^0$, dark blue dashed curve) is mainly observed from approximately 10^{11} to 10^{15} eV, while proton-driven SSC processes (black curve) are significant from 10^6 to 10^{16} eV.

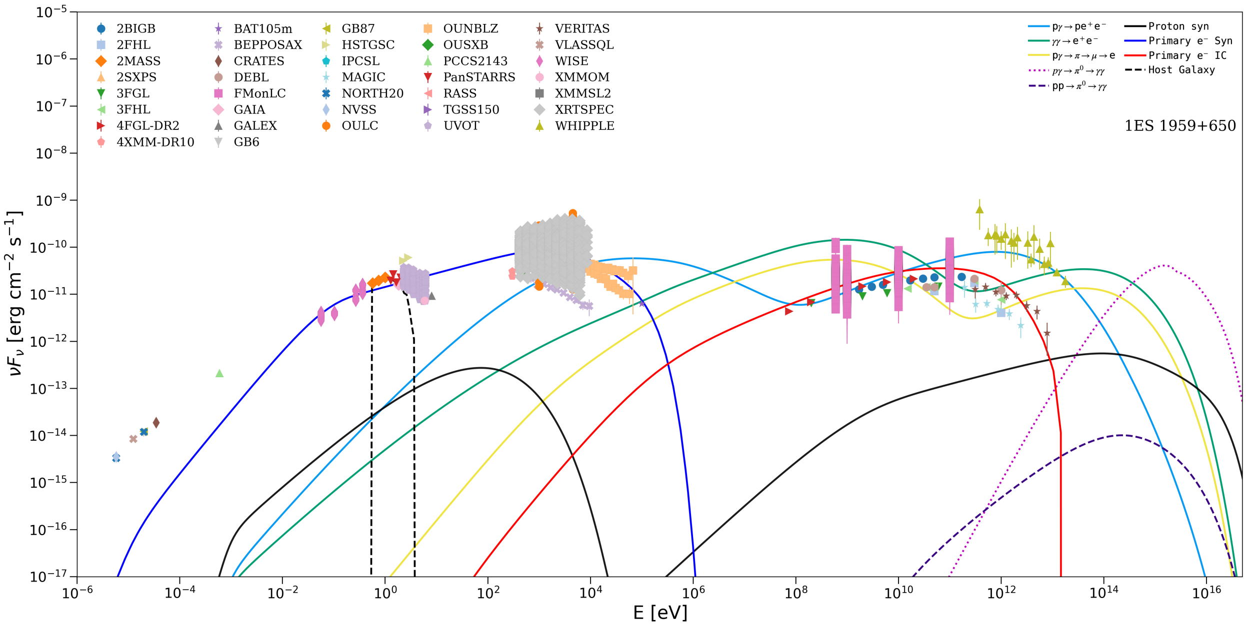

Figure 4. Lepto-hadronic SED modeling and multi-wavelength data of 1ES 1959+650 (see Table 2 for detailed observatory data used in the modeling). In comparison to the purely leptonic model, the lepto-hadronic model is characterized by the dominant contributions to the emissions of high-energy photons and neutrinos. These processes originate from the following interactions: proton–photon interactions ($p\gamma$, purple dotted curve) are observed from 10^{11} eV to 10^{17} eV. Pion production from proton–proton interactions ($pp \rightarrow \pi^0$, dark blue dashed curve) is mainly observed from approximately 10^{11} to 10^{15} eV, while proton-driven SSC processes (black curve) are significant from 10^6 to 10^{16} eV.

In Figure 3, the model suggests a possible hadronic contribution within the energy range of 10^8 to 2×10^{12} eV. In this scenario, Bethe–Heitler pair production, arising from the interaction of ultra-high-energy protons with ambient photon fields, generates secondary electron–positron pairs that undergo IC scattering. These IC interactions upscatter low-energy ambient photons into the gamma-ray regime, producing the high-energy bump seen in the light blue curve, which matches the gamma-ray flux of 1.78×10^{-11} erg cm^{-2} s^{-1} at 1.08×10^{12} eV, as reported in the 2FHL catalog by *Fermi*-LAT [98]. Additionally, a lower energy flux of 5.2×10^{-12} erg cm^{-2} s^{-1} at approximately 0.2 GeV, detected by *Fermi*-LAT (Fermi 1FGL catalog) [95], can be attributed either to synchrotron emission by secondary electrons from muon decay, originating from pion decay in proton-photon interactions, or possibly to inverse Compton scattering by electrons produced in Bethe–Heitler pair production. Both data points are highlighted with dashed-line circles in the figure. Thus, emissions from both Bethe–Heitler pairs and secondary electrons from muon decay contribute significantly to the broadband emission of the source, offering a coherent and self-consistent interpretation of the multiwavelength observations.

In Figure 4, the model indicates a potential hadronic contribution that fills the "gap" between the two characteristic broadband emission features. In this scenario, Bethe–Heitler pair production by ultra-high-energy protons accounts for the X-ray fluxes observed in this intermediate region. These X-ray emissions originate from synchrotron radiation produced by secondary electron–positron pairs generated through the Bethe–Heitler process. Additionally, the IC component, represented by the high-energy bump in the same light blue curve, contributes significantly to explaining the observational data between approximately 10^{11} eV and 10^{14} eV. This energy range corresponds to VHE gamma-rays detected during flaring activity by the Whipple observatory. Notably, on 4 June 2002, the source exhibited a dramatic gamma-ray flare without a simultaneous increase in the X-ray band, marking the first clear detection of an "orphan" gamma-ray flare from a blazar [130]. The analysis of such sources underscores the necessity of adopting a lepto-hadronic framework to fully account for their high-energy emission behavior. This approach has important implications, as it suggests the potential for future neutrino detections and provides strong support for the existence of nuclear acceleration processes in these environments [131–134].

5. Conclusions

We employed the open-source softwares JetSeT and AM^3 to model the SEDs of two high-frequency peaked BL Lac (HBL) sources: 1ES 0414+009 and 1ES 1959+650. We determined the best-fit model parameters by matching the predicted multiwavelength emission to publicly available observational data for both sources. Initial modeling using a purely leptonic scenario yielded fits that could not adequately reproduce the observed hard gamma-ray spectra during flaring states, particularly above 10^{11} eV. We therefore extended our analysis to a lepto-hadronic model, incorporating proton-proton (pp) and proton-photon ($p\gamma$) interactions within the jet environment. The inclusion of the $p\gamma$ component indicates that hadronic processes may contribute significantly in the high-energy emission of these two HBLs during flaring episodes. For both sources, Bethe–Heitler pair production ($p\gamma \to p + e^+ + e^-$) by ultra-high-energy protons plays a key role in shaping the high-energy emission. In 1ES 1959+650, secondary electron–positron pairs generated through this process produce synchrotron radiation that accounts for the X-ray fluxes observed in the intermediate energy range, while their IC scattering of ambient photons contributes to the VHE gamma-ray emission. In 1ES 0414+009, the VHE gamma-ray flux can likewise be partially attributed to IC scattering by Bethe–Heitler secondaries. Thus, in both cases, Bethe–Heitler pair production injects relativistic leptons into the emission region, where they radiate via synchrotron and/or IC processes. These contributions complement the emission from primary electrons and offer a coherent explanation for the broadband spectral features observed during flaring episodes. In conclusion, the lepto-hadronic framework effectively reproduces the multiwavelength observations across a broad energy spectrum for the two sources, underscoring the importance of incorporating hadronic processes to achieve a comprehensive understanding of BL Lac emission.

Author Contributions: Conceptualization, L.A.S.P.; methodology, S.V.B.d.S. and L.A.S.P.; software, S.V.B.d.S.; formal analysis, S.V.B.d.S.; investigation, S.V.B.d.S., L.A.S.P. and R.d.C.D.A.; resources, L.A.S.P. and R.d.C.D.A.; data curation, S.V.B.d.S. and L.A.S.P.; writing—original draft preparation, S.V.B.d.S., L.A.S.P. and R.d.C.D.A.; writing—review and editing, S.V.B.d.S., L.A.S.P. and R.d.C.D.A.; visualization, S.V.B.d.S., L.A.S.P. and R.d.C.D.A.; supervision, L.A.S.P.; project administration, L.A.S.P.; funding acquisition, L.A.S.P. and R.d.C.D.A. All authors have read and agreed to the published version of the manuscript.

Funding: Stuani Pereira, L.A. gratefully acknowledges financial support from FAPESP under grant numbers 2021/01089-1, 2024/02267-9 and 2024/14769-9 and CNPq under grant numbers 403337/2024-0, 153839/2024-4 and 200164/2025-2. dos Anjos, R.C. acknowledges the financial support from the NAPI "Fenômenos Extremos do Universo" of Fundação de Apoio à Ciência, Tecnologia e Inovação do Paraná. R.C.A.'s research is supported by the CAPES/Alexander von Humboldt Program (88881.800216/2022-01), Conselho Nacional de Desenvolvimento Científico e Tecnológico (CNPq) grant numbers (307750/2017-5) and (401634/2018-3/AWS), Araucária Foundation (698/2022) and (721/2022), and FAPESP (2021/01089-1). She also thanks L'Oreal Brazil for the support, with the partnership of ABC and UNESCO in Brazil. The authors acknowledge the National Laboratory for Scientific Computing (LNCC/MCTI, Brazil) for providing HPC resources through the SDumont supercomputer, which significantly supported the computational aspects of this research, which have contributed to the research results reported in this paper. URL: https://sdumont.lncc.br accessed on 28 May 2025.

Data Availability Statement: The original contributions presented in this study are included in the article. Further inquiries can be directed to the corresponding authors.

Conflicts of Interest: The authors declare no conflicts of interest.

Abbreviations

The following abbreviations are used in this manuscript:

AGNs	Active Galactic Nuclei
FSRQ	flat-spectrum radio quasar
AGN	Active Galactic Nuclei
FSRQ	Flat-Spectrum Radio Quasar
BLO	BL Lac Object
SED	Spectral Energy Distribution
LBL	Low-Frequency Peaked BL Lac
IBL	Intermediate-Frequency Peaked BL Lac
HBL	High-Frequency Peaked BL Lac
EHBL	Extreme High-Frequency Peaked BL Lac
Syn	Synchrotron
IC	Inverve Compton
EC	External Compton
BLR	Broad-Line Region
DT	Dusty Torus
SMBH	Supermassive Black Hole
CMB	Cosmic Microwave Background
EBL	Extragalactic Background Light
SSC	Synchrotron Self-Compton
MCMC	Markov Chain Monte Carlo
SSDC	Space Science Data Center
HE	High-Energy
VHE	Very High-Energy

Notes

[1] https://www.ssdc.asi.it/, accessed on 1 February 2025.

[2] https://firmamento.hosting.nyu.edu/home, accessed on 1 February 2025.

References

1. Urry, C.M.; Padovani, P. Unified Schemes for Radio-Loud Active Galactic Nuclei. *Astron. Soc. Pac.* **1995**, *107*, 803–891. [CrossRef]
2. Wills, B.J.; Wills, D.; Breger, M.; Antonucci, R.R.J.; Barvainis, R. A Survey for High Optical Polarization in Quasars with Core-dominant Radio Structure: Is There a Beamed Optical Continuum? *Astrophys. J.* **1992**, *398*, 454–475. [CrossRef]
3. Ghisellini, G.; Tavecchio, F.; Foschini, L.; Ghirlanda, G.; Maraschi, L.; Celotti, A. General physical properties of bright Fermi blazars. *Mon. Not. R. Astron. Soc.* **2010**, *402*, 497–518. [CrossRef]
4. Kang, S.J.; Chen, L.; Wu, Q. Constraints on the minimum electron lorentz factor and matter content of jets for a sample of bright Fermi blazars. *Astrophys. J. Suppl. Ser.* **2014**, *215*, 5. [CrossRef]
5. Fan, J.H.; Yang, J.H.; Liu, Y.; Luo, G.Y.; Lin, C.; Yuan, Y.H.; Xiao, H.B.; Zhou, A.Y.; Hua, T.X.; Pei, Z.Y. The spectral energy distributions of Fermi blazars. *Astrophys. J. Suppl. Ser.* **2016**, *226*, 20. [CrossRef]
6. Yang, J.H.; Fan, J.H.; Liu, Y.; Tuo, M.X.; Pei, Z.Y.; Yang, W.X.; Yuan, Y.H.; He, S.L.; Wang, S.H.; Wang, X.C.; et al. The Spectral Energy Distributions for 4FGL Blazars. *Astrophys. J. Suppl. Ser.* **2022**, *262*, 18. [CrossRef]
7. Cao, G.; Wang, J. The Hadronic Origin of the Hard Gamma-Ray Spectrum from Blazar 1ES 1101-232. *Astrophys. J.* **2014**, *783*, 108–110. [CrossRef]
8. Abdo, A.A.; Ackermann, M.; Agudo, I.; Ajello, M.; Aller, H.D.; Aller, M.F.; Angelakis, E.; Arkharov, A.A.; Axelsson, M.; Bach, U.; et al. The spectral energy distribution of Fermi bright blazars. *Astrophys. J.* **2010**, *716*, 30. [CrossRef]
9. Zhou, R.X.; Zheng, Y.G.; Zhu, K.R.; Kang, S.J. The Intrinsic Properties of Multiwavelength Energy Spectra for Fermi Teraelectron-volt Blazars. *Astrophys. J.* **2021**, *915*, 59. [CrossRef]

10. Zhou, R.X.; Zheng, Y.G.; Zhu, K.R.; Kang, S.J.; Li, X.P. Modeling the Multiwavelength Spectral Energy Distributions of the Fermi-4LAC Bright Flat-spectrum Radio Quasars. *Astrophys. J.* **2024**, *962*, 22. [CrossRef]
11. Hu, H.B.; Wang, H.Q.; Xue, R.; Peng, F.K.; Wang, Z.R. The physical properties of Fermi-4LAC low-synchrotron-peaked BL Lac objects. *Mon. Not. R. Astron. Soc.* **2024**, *528*, 7587–7599. [CrossRef]
12. Tavecchio, F.; Ghisellini, G.; Ghirlanda, G.; Foschini, L.; Maraschi, L. TeV BL Lac objects at the dawn of the Fermi era. *Mon. Not. R. Astron. Soc.* **2010**, *401*, 1570–1586. [CrossRef]
13. Zheng, Y.G.; Long, G.B.; Yang, C.Y.; Bai, J.M. Verification of the diffusive shock acceleration in Mrk 501. *Mon. Not. R. Astron. Soc.* **2018**, *478*, 3855–3861. [CrossRef]
14. Dermer, C.D.; Schlickeiser, R. Model for the High-Energy Emission from Blazars. *Astrophys. J.* **1993**, *416*, 458–484. [CrossRef]
15. Sikora, M.; Begelman, M.C.; Rees, M.J. Comptonization of Diffuse Ambient Radiation by a Relativistic Jet: The Source of Gamma Rays from Blazars? *Astrophys. J.* **1994**, *421*, 153–162. [CrossRef]
16. Aharonian, F.A. TeV gamma rays from BL Lac objects due to synchrotron radiation of extremely high energy protons. *New Astronomy.* **2000**, *5*, 377–395. [CrossRef]
17. Mücke, A.; Protheroe, R.J.; Engel, R.; Rachen, J.P.; Stanev, T. BL Lac objects in the synchrotron proton blazar model. *Astropart. Phys.* **2003**, *18*, 593–613. [CrossRef]
18. Petropoulou, M. The role of hadronic cascades in GRB models of efficient neutrino production. *Mthly. Not. R. Astron. Soc.* **2014**, *442*, 3026–3036. [CrossRef]
19. Mannheim, K.; Biermann, P.L. Gamma-ray flaring of 3C 279: A proton-initiated cascade in the jet? *Astron. Astrophys.* **1992**, *253*, L21–L24.
20. Mannheim, K. The proton blazar. *Astron. Astrophys.* **1993**, *269*, 67–76. [CrossRef]
21. Pohl, M.; Schlickeiser, R. On the conversion of blast wave energy into radiation in active galactic nuclei and gamma-ray bursts. *Astron. Astrophys.* **2000**, *354*, 395–410. [CrossRef]
22. Atoyan, A.; Dermer, C.D. High-Energy Neutrinos from Photomeson Processes in Blazars. *Physical. Rev. Lett.* **2001**, *87*, 221102–221105. [CrossRef] [PubMed]
23. Zhang, J.; Liang, E.W.; Zhang, S.N.; Bai, J.M. Radiation mechanisms and physical properties of GeV–TeV BL Lac objects. *Astrophys. J.* **2012**, *752*, 157. [CrossRef]
24. Fan, J.; Xiao, H.; Yang, W.; Zhang, L.; Strigachev, A.A.; Bachev, R.S.; Yang, J. Characterizing the Emission Region Properties of Blazars. *Astrophys. J. Suppl. Ser.* **2023**, *268*, 23. [CrossRef]
25. Blandford, R.D.; Znajek, R.L. Electromagnetic extraction of energy from Kerr black holes. *Mon. Not. R. Astron. Soc.* **1977**, *179*, 433–456. [CrossRef]
26. Blandford, R.D.; Payne, D.G. Hydromagnetic flows from accretion discs and the production of radio jets. *Mon. Not. R. Astron. Soc.* **1982**, *199*, 883–903. [CrossRef]
27. Maraschi, L.; Tavecchio, F. The Jet-Disk Connection and Blazar Unification. *Astrophys. J.* **2003**, *593*, 667. [CrossRef]
28. Zhao, X.Z.; Yang, H.Y.; Zheng, Y.G.; Kang, S.J. The Energy Budget in the Jet of High-frequency Peaked BL Lacertae Objects *Astrophys. J.* **2024**, *967*, 104. [CrossRef]
29. Sironi, L.; Petropoulou, M.; Giannios, D. Relativistic jets shine through shocks or magnetic reconnection? *Mon. Not. R. Astron. Soc.* **2015**, *450*, 183–191. [CrossRef]
30. Lobanov, A.P. Ultracompact jets in AGN. *Astron. Astrophys.* **1998**, *330*, 79–90.
31. Zamaninasab, M.; Clausen-Brown, E.; Savolainen, T.; Tchekhovskoy, A. Dynamically important magnetic fields near accreting supermassive black holes. *Nature* **2014**, *510*, 126–128. [CrossRef] [PubMed]
32. Ghisellini, G.; Celotti, A.; Fossati, G.; Maraschi, L.; Comastri, A. A theoretical unifying scheme for gamma-ray bright blazars. *Mon. Not. R. Astron. Soc.* **1998**, *301*, 451–468. [CrossRef]
33. Tavecchio, F.; Maraschi, L.; Ghisellini, G. Constraints on the Physical Parameters of TeV Blazars. *Astrophys. J.* **1998**, *509*, 608. [CrossRef]
34. Tavecchio, F.; Ghisellini, G.; Bonnoli, G.; Ghirlanda, G. Constraining the location of the emitting region in Fermi blazars through rapid γ-ray variability. *Mon. Not. R. Astron. Soc. Lett.* **2010**, *405*, L94–L98. [CrossRef]
35. Sol, H.; Zech, A. Blazars at Very High Energies: Emission Modelling. *Galaxies* **2022**, *10*, 105. [CrossRef]
36. Kelner, S.R.; Aharonian, F.A. Energy spectra of gamma rays, electrons, and neutrinos produced at interactions of relativistic protons with low energy radiation. *Phys. Rev. D* **2008**, *78*, 034013–034028. [CrossRef]
37. Karavola, D.; Petropoulou, M. A closer look at the electromagnetic signatures of Bethe-Heitler pair production process in blazars. *J. Cosmol. Astropart. Phys.* **2024**, *2024*, 6–55. [CrossRef]
38. Gursky, H.; Bradt, H.; Doxsey, R.; Schwartz, D.; Schwarz, J.; Dower, R.; Fabbiano, G.; Griffiths, R.E.; Johnston, M.; Leach, R.; et al. Measurements of X-ray source positions by the scanning modulation collimator on HEAO 1. *Astrophys. J.* **1978**, *223*, 973–978. [CrossRef]

39. Giacconi, R.; Branduardi, G.; Briel, U.; Epstein, A.; Fabricant, D.; Feigelson, E.; Forman, W.; Gorenstein, P.; Grindlay, J.; Gursky, H.; et al. The Einstein (HEAO 2) X-ray Observatory. *Astrophys. J.* **1979**, *230*, 540–550. [CrossRef]
40. Halpern, J.P.; Chen, V.S.; Madejski, G.M.; Chanan, G.A. The Redshift of the X-ray Selected BL Lacertae Object H0414+009. *Astron. J.* **1991**, *101*, 818. [CrossRef]
41. Falomo, R.; Carangelo, N.; Treves, A. Host galaxies and black hole masses of low- and high-luminosity radio-loud active nuclei. *Mthly. Not. R. Astron. Soc.* **2003**, *343*, 505–511. [CrossRef]
42. Padovani, P.; Giommi, P. A sample-oriented catalogue of BL Lacertae objects. *Mthly. Not. R. Astron. Soc.* **1995**, *277*, 1477–1490. [CrossRef]
43. Aharonian, F.A.; Akhperjanian, A.G.; Barrio, J.A.; Bernlöhr, K.; Bojahr, H.; Calle, I.; Contreras, J.L.; Cortina, J.; Daum, A.; Deckers, T.; et al. HEGRA search for TeV emission from BL Lacertae objects. *Astronomy. Astrophys.* **2000**, *353*, 847–852. [CrossRef]
44. Costamante, L.; Ghisellini, G. TeV candidate BL Lac objects. *Astronomy. Astrophys.* **2002**, *384*, 56–71. [CrossRef]
45. Aharonian, F.; Akhperjanian, A.G.; Bazer-Bachi, A.R.; Beilicke, M.; Benbow, W.; Berge, D.; Bernlöhr, K.; Boisson, C.; Bolz, O.; Borrel, V.; et al. A low level of extragalactic background light as revealed by γ-rays from blazars. *Nature* **2006**, *440*, 1018–1021. [CrossRef]
46. Volpe, F.; Ohm, S.; Hauser, M.; Kaufmann, S.; Gérard, L.; Costamante, L.; Fegan, S.; Ajello, M. Discovery of VHE and HE emission from the blazar 1ES 0414+009 with H.E.S.S and Fermi-LAT. *arXiv* **2011**, arXiv:1105.5114.
47. Abramowski, A.; Acero, F.; Aharonian, F.; Akhperjanian, A.; Anton, G.; Balzer, A.; Barnacka, A.; De Almeida, U.B.; Becherini, Y.; Becker, J.; et al. Discovery of hard-spectrum γ-ray emission from the BL Lacertae object 1ES 0414+ 009. *Astron. Astrophys.* **2012**, *538*, A103.
48. Zhang, B.; Zhao, X.; Cao, Z. TeV Blazars as the Sources of Ultra High Energy Cosmic Rays. *Int. J. Astron. Astrophys.* **2014**, *4*, 499–509. [CrossRef]
49. Acciari, V.A.; Ansoldi, S.; Antonelli, L.A.; Engels, A.A.; Asano, K.; Baack, D.; Babić, A.; Banerjee, B.; Barres de Almeida, U.; Barrio, J.A.; et al. New Hard-TeV Extreme Blazars Detected with the MAGIC Telescopes. *Astrophys. J.* **2020**, *247*, 16–39. [CrossRef]
50. Piner, B.G.; Edwards, P.G. First-Epoch VLBA Imaging of 20 New TeV Blazars. *Astrophys. J.* **2014**, *797*, 25–40. [CrossRef]
51. Pueschel, E. The Extragalactic Background Light: Constraints from TeV Blazar Observations. *Proc. Sci.* **2017**, *ICRC2017*, 1107. [CrossRef]
52. Elvis, M.; Plummer, D.; Schachter, J.; Fabbiano, G. The Einstein slew survey. *Astrophys. J.* **1992**, *80*, 257–303. [CrossRef]
53. Schachter, J.F.; Stocke, J.T.; Perlman, E.; Elvis, M.; Remillard, R.; Granados, A.; Luu, J.; Huchra, J.P.; Humphreys, R.; Urry, C.M.; et al. Ten New BL Lacertae Objects Discovered by an Efficient X-Ray/Radio/Optical Technique. *Astrophys. J.* **1993**, *412*, 541. [CrossRef]
54. Nishiyama, T.; Chamoto, N.; Chikawa, M. Detection of a new TeV gamma-ray source of BL Lac object 1ES 1959+650. In Proceedings of the 26th International Cosmic-Ray Conference, Salt Lake City, UT, USA, 17–25 August 1999.
55. Holder, J.; Bond, I.H.; Boyle, P.J.; Bradbury, S.M.; Buckley, J.H.; Carter-Lewis, D.A.; Cui, W.; Dowdall, C.; Duke, C.; de la Calle Perez, I.; et al. Detection of TeV Gamma Rays from the BL Lacertae Object 1ES 1959+650 with the Whipple 10 Meter Telescope. *Astrophys. J.* **2002**, *583*, L9. [CrossRef]
56. Horns, D. Multi-wavelength Observations of the TeV Blazars Mkn 421, 1ES1959+650, and H1426+428 with the HEGRA Cherenkov Telescopes and the RXTE X-ray Satellite. In *High Energy Blazar Astronomy*; Takalo, L.O., Valtaoja, E., Eds.; Astronomical Society of the Pacific Conference Series; Astronomical Society of the Pacific Conference Series; Astronomical Society of the Pacific: San Francisco, CA, USA, 2003; Volume 299, p. 13. [CrossRef]
57. Aharonian, F.; Akhperjanian, A.; Beilicke, M.; Bernlöhr, K.; Börst, H.G.; Bojahr, H.; Bolz, O.; Coarasa, T.; Contreras, J.L.; Cortina, J.; et al. Detection of TeV gamma-rays from the BL Lac 1ES 1959+650 in its low states and during a major outburst in 2002. *Astronomy. Astrophys.* **2003**, *406*, L9–L13. [CrossRef]
58. Kapanadze, B.; Dorner, D.; Romano, P.; Vercellone, S.; Tabagari, L. The TeV blazar 1ES 1959+650—A short review. *Proc. Sci.* **2018**, *4*, 33. [CrossRef]
59. Aliu, E.; Archambault, S.; Arlen, T.; Aune, T.; Beilicke, M.; Benbow, W.; Bird, R.; Böttcher, M.; Bouvier, A.; Bugaev, V.; et al. Multiwavelength Observations and Modeling of 1ES 1959+650 in a Low Flux State. *Astrophys. J.* **2013**, *775*, 3–11. [CrossRef]
60. Aliu, E.; Archambault, S.; Arlen, T.; Aune, T.; Barnacka, A.; Beilicke, M.; Benbow, W.; Berger, K.; Bird, R.; Bouvier, A.; et al. Investigating Broadband Variability of the TeV Blazar 1ES 1959+650. *Astrophys. J.* **2014**, *797*, 89–99. [CrossRef]
61. Kapanadze, B.; Romano, P.; Vercellone, S.; Kapanadze, S.; Mdzinarishvili, T.; Kharshiladze, G. The long-term Swift observations of the high-energy peaked BL Lacertae source 1ES 1959+650. *Mon. Not. R. Astron. Soc.* **2016**, *457*, 704–722. [CrossRef]
62. Kapanadze, B.; Dorner, D.; Vercellone, S.; Romano, P.; Kapanadze, S.; Mdzinarishvili, T. A recent strong X-ray flaring activity of 1ES 1959+650 with possibly less efficient stochastic acceleration. *Mon. Not. R. Astron. Soc.* **2016**, *461*, L26–L31. [CrossRef]
63. Kapanadze, B.; Dorner, D.; Vercellone, S.; Romano, P.; Hughes, P.; Aller, M.; Aller, H.; Reynolds, M.; Kapanadze, S.; Tabagari, L. The second strong X-ray flare and multifrequency variability of 1ES 1959+650 in 2016 January-August. *Mon. Not. R. Astron. Soc.* **2018**, *473*, 2542–2564. [CrossRef]

64. Shukla, A.; Chitnis, V.R.; Singh, B.B.; Acharya, B.S.; Anupama, G.C.; Bhattacharjee, P.; Britto, R.J.; Mannheim, K.; Prabhu, T.P.; Saha, L.; et al. Multi-frequency, multi-epoch study of Mrk 501: Hints for a two-component nature of the emission. *Astrophys. J.* **2014**, *798*, 2. [CrossRef]
65. Tramacere, A.; Giommi, P.; Perri, M.; Verrecchia, F.; Tosti, G. Swift observations of the very intense flaring activity of Mrk 421 during 2006. I. Phenomenological picture of electron acceleration and predictions for MeV/GeV emission. *Astronomy. Astrophys.* **2009**, *501*, 879–898. [CrossRef]
66. Tramacere, A.; Massaro, E.; Taylor, A.M. Stochastic Acceleration and the Evolution of Spectral Distributions in Synchro-Self-Compton Sources: A Self-consistent Modeling of Blazars' Flares. *Astrophys. J.* **2011**, *739*, 66–81. [CrossRef]
67. Tramacere, A. *JetSeT: Numerical Modeling and SED Fitting Tool for Relativistic Jets*; record ascl:2009.001; Astrophysics Source Code Library: College Park, MD, USA, 2020.
68. Dominguez, A.; Primack, J.R.; Rosario, D.J.; Prada, F.; Gilmore, R.C.; Faber, S.M.; Koo, D.C.; Somerville, R.S.; Perez-Torres, M.A.; Perez-Gonzalez, P.; et al. Extragalactic Background Light Inferred from AEGIS Galaxy SED-type Fractions. *Mon. Not. Roy. Astron. Soc.* **2011**, *410*, 2556–2579. [CrossRef]
69. Franceschini, A.; Rodighiero, G.; Vaccari, M. The extragalactic optical-infrared background radiations, their time evolution and the cosmic photon-photon opacity. *Astron. Astrophys.* **2008**, *487*, 837–852. [CrossRef]
70. Finke, J.D.; Razzaque, S.; Dermer, C.D. Modeling the Extragalactic Background Light from Stars and Dust. *Astrophys. J.* **2010**, *712*, 238–249. [CrossRef]
71. Ghisellini, G.; Tavecchio, F.; Maraschi, L.; Celotti, A.; Sbarrato, T. The power of relativistic jets is larger than the luminosity of their accretion disks. *Nature* **2014**, *515*, 376–395. [CrossRef]
72. Fan, J.-H.; Yang, J.H.; Liu, Y.; Zhang, J.-Y. The gamma-ray Doppler factor determinations for a Fermi blazar sample. *Res. Astron. Astrophys.* **2013**, *13*, 259. [CrossRef]
73. Nalewajko, K. The brightest gamma-ray flares of blazars. *Mon. Not. R. Astron. Soc.* **2013**, *430*, 1324–1333. [CrossRef]
74. Dembinski, H.; Ongmongkolkul, P.; Deil, C.; Schreiner, H.; Feickert, M.; Burr, C.; Watson, J.; Rost, F.; Pearce, A.; Geiger, L.; et al. *Scikit-Hep/Iminuit*; Zenodo: Geneva, Switzerland, 2024. Available online:. (accessed on 30 May 2025). [CrossRef]
75. Virtanen, P.; Gommers, R.; Oliphant, T.E.; Haberland, M.; Reddy, T.; Cournapeau, D.; Burovski, E.; Peterson, P.; Weckesser, W.; Bright, J.; et al. SciPy 1.0: Fundamental Algorithms for Scientific Computing in Python. *Nat. Methods* **2020**, *17*, 261–272. [CrossRef]
76. Foreman-Mackey, D.; Hogg, D.W.; Lang, D.; Goodman, J. emcee: The MCMC Hammer. *Astron. Soc. Pac.* **2013**, *125*, 306–312. [CrossRef]
77. Ghisellini, G. Electron—Positron pairs in blazar jets and γ-ray loud radio galaxies. *Mon. Not. R. Astron. Soc. Lett.* **2012**, *424*, L26–L30. [CrossRef]
78. Klinger, M.; Rudolph, A.; Rodrigues, X.; Yuan, C.; de Clairfontaine, G.F.; Fedynitch, A.; Winter, W.; Pohl, M.; Gao, S. AM^3: An Open-source Tool for Time-dependent Lepto-hadronic Modeling of Astrophysical Sources. *Astrophys. J. Suppl.* **2024**, *275*, 4–26. [CrossRef]
79. Hümmer, S.; Rüger, M.; Spanier, F.; Winter, W. Simplified models for photohadronic interactions in cosmic accelerators. *Astrophys. J.* **2010**, *721*, 630. [CrossRef]
80. White, R.L.; Becker, R.H. A New Catalog of 30,239 1.4 GHz Sources. *Astrophys. J. Suppl. Ser.* **1992**, *79*, 331. [CrossRef]
81. Condon, J.J.; Cotton, W.D.; Greisen, E.W.; Yin, Q.F.; Perley, R.A.; Taylor, G.B.; Broderick, J.J. The NRAO VLA Sky Survey. *Astron. J.* **1998**, *115*, 1693–1716. [CrossRef]
82. Healey, S.E.; Romani, R.W.; Taylor, G.B.; Sadler, E.M.; Ricci, R.; Murphy, T.; Ulvestad, J.S.; Winn, J.N. CRATES: An All-Sky Survey of Flat-Spectrum Radio Sources. *Astrophys. J.* **2007**, *171*, 61. [CrossRef]
83. Myers, S.T.; Jackson, N.J.; Browne, I.W.A.; de Bruyn, A.G.; Pearson, T.J.; Readhead, A.C.S.; Wilkinson, P.N.; Biggs, A.D.; Blandford, R.D.; Fassnacht, C.D.; et al. The Cosmic Lens All-Sky Survey: Survey Selection and Images. *Astrophys. J.* **2003**, *591*, 575. [CrossRef]
84. Griffith, M.R.; Wright, A.E. The Parkes-MIT-NRAO (PMN) surveys. I. *Astron. J.* **1993**, *105*, 1666.
85. Gregory, P.C.; Scott, W.K.; Douglas, K.; Condon, J.J. The GB6 catalog of radio sources. *Astrophys. J. Suppl. Ser.* **1996**, *103*, 427–432. [CrossRef]
86. Taylor, B.G.; Andresen, R.D.; Peacock, A.; Zobl, R. The EXOSAT mission. *Space Sci. Rev.* **1986**, *40*, 391–420.
87. Wright, A.E.; Griffith, M.R.; Troup, E.; Hunt, A.J.; Burke, B. The Parkes-MIT-NRAO (PMN) Surveys. VIII: Source Catalog for the Zenith Survey ($-37.0 < d < -29.0$). *Astrophys. J.* **1997**, *103*, 145.
88. Boller, T.; Freyberg, M.; Trümper, J.; Haberl, F.; Voges, W.; Nandra, K. Second ROSAT all-sky survey (2RXS) source catalogue. *Astron. Astrophys.* **2016**, *588*, A103. [CrossRef]
89. Voges, W.; Aschenbach, B.; Boller, T.; Braeuninger, H.; Briel, U.; Burkert, W.; Dennerl, K.; Englhauser, J.; Gruber, R.; Haberl, F.; et al. The ROSAT all-sky survey bright source catalogue. *Astron. Astrophys.* **1999**, *349*, 389–405.
90. Levine, A.; Lang, F.; Lewin, W.; Primini, F.; Dobson, C.; Doty, J.; Hoffman, J.; Howe, S.; Scheepmaker, A.; Wheaton, W.; et al. The HEAO 1 A-4 catalog of high-energy X-ray sources. *Astrophys. J. Suppl. Ser.* **1984**, *54*, 581–617. [CrossRef]

91. Evans, P.A.; Beardmore, A.P.; Page, K.L.; Osborne, J.P.; O'Brien, P.T.; Willingale, R.; Starling, R.L.C.; Burrows, D.N.; Godet, O.; Vetere, L.; et al. Methods and results of an automatic analysis of a complete sample of Swift-XRT observations of GRBs. *Astron. Astrophys.* **2007**, *469*, 379–385. [CrossRef]
92. Evans, P.A.; Osborne, J.P.; Beardmore, A.P.; Page, K.L.; Willingale, R.; Mountford, C.J.; Pagani, C.; Burrows, D.N.; Kennea, J.A.; Perri, M.; et al. 1SXPS: A deep Swift X-ray telescope point source catalog. *Astrophys. J.* **2014**, *210*, 8. [CrossRef]
93. Giommi, P.; Capalbi, M.; Fiocchi, M.; Memola, E.; Perri, M.; Piranomonte, S.; Rebecchi, S.; Massaro, E. A catalog of 157 X-ray spectra and 84 spectral energy distributions of blazars observed with BeppoSAX. In *Blazar Astrophysics with BeppoSAX and Other Observatories*; ESA-ESRIN: Frascati, Italy, 2002. [CrossRef]
94. Ackermann, M.; Ajello, M.; Atwood, W.B.; Baldini, L.; Ballet, J.; Barbiellini, G.; Bastieri, D.; Gonzalez, J.B.; Bellazzini, R.; Bissaldi, E.; et al. The third catalog of active galactic nuclei detected by the fermi large area telescope. *Astrophys. J.* **2015**, *810*, 14. [CrossRef]
95. Abdo, A.A.; Ackermann, M.; Ajello, M.; Allafort, A.; Antolini, E.; Atwood, W.; Axelsson, M.; Baldini, L.; Ballet, J.; Barbiellini, G.; et al. Fermi large area telescope first source catalog. *Astrophys. J. Suppl. Ser.* **2010**, *188*, 405. [CrossRef]
96. Nolan, P.L.; Abdo, A.; Ackermann, M.; Ajello, M.; Allafort, A.; Antolini, E.; Atwood, W.; Axelsson, M.; Baldini, L.; Ballet, J.; et al. Fermi large area telescope second source catalog. *Astrophys. J. Suppl. Ser.* **2012**, *199*, 31. [CrossRef]
97. Acero, F.; Ackermann, M.; Ajello, M.; Albert, A.; Atwood, W.; Axelsson, M.; Baldini, L.; Ballet, J.; Barbiellini, G.; Bastieri, D.; et al. Fermi large area telescope third source catalog. *Astrophys. J. Suppl. Ser.* **2015**, *218*, 23. [CrossRef]
98. Ackermann, M.; Ajello, M.; Atwood, W.B.; Baldini, L.; Ballet, J.; Barbiellini, G.; Bastieri, D.; Gonzalez, J.B.; Bellazzini, R.; Bissaldi, E.; et al. 2FHL: The second catalog of hard Fermi-LAT sources. *Astrophys. J. Suppl. Ser.* **2016**, *222*, 5. [CrossRef]
99. Abdollahi, S.; Acero, F.; Baldini, L.; Ballet, J.; Bastieri, D.; Bellazzini, R.; Berenji, B.; Berretta, A.; Bissaldi, E.; Blandford, R.D.; et al. Incremental fermi large area telescope fourth source catalog. *Astrophys. J. Suppl. Ser.* **2022**, *260*, 53. [CrossRef]
100. Johnston, C. One size does not fit all: Evidence for a range of mixing efficiencies in stellar evolution calculations. *Astron. Astrophys.* **2021**, *655*, A29. [CrossRef]
101. Bartoli, B.; Bernardini, P.; Bi, X.J.; Bolognino, I.; Branchini, P.; Budano, A.; Calabrese Melcarne, A.K.; Camarri, P.; Cao, Z.; Cardarelli, R.; et al. TeV gamma-ray survey of the northern sky using the ARGO-YBJ detector. *Astrophys. J.* **2013**, *779*, 27. [CrossRef]
102. Aliu, E.; Archambault, S.; Arlen, T.; Aune, T.; Beilicke, M.; Benbow, W.; Boettcher, M.; Bouvier, A.; Bugaev, V.; Cannon, A.; et al. Multiwavelength observations of the AGN 1ES 0414+ 009 with VERITAS, Fermi-LAT, Swift-XRT, and MDM. *Astrophys. J.* **2012**, *755*, 118. [CrossRef]
103. Skrutskie, M.F.; Cutri, R.M.; Stiening, R.; Weinberg, M.D.; Schneider, S.; Carpenter, J.M.; Beichman, C.; Capps, R.; Chester, T.; Elias, J.; et al. The Two Micron All Sky Survey (2MASS). *Astron. J.* **2006**, *131*, 1163. [CrossRef]
104. Cutri, R.; Wright, E.; Conrow, T.; Fowler, J.W.; Eisenhardt, P.R.M.; Grillmair, C.; Kirkpatrick, J.D.; Masci, F.; McCallon, H.L.; Wheelock, S.L.; et al. *VizieR On-line Data Catalog: II/328*; Caltech: Pasadena, CA, USA, 2013.
105. Akrami, Y.; Argüeso, F.; Ashdown, M.; Aumont, J.; Baccigalupi, C.; Ballardini, M.; Banday, A.J.; Barreiro, R.; Bartolo, N.; Basak, S.; et al. Planck intermediate results-LIV. The Planck multi-frequency catalogue of non-thermal sources. *Astron. Astrophys.* **2018**, *619*, A94.
106. Intema, H.T.; Jagannathan, P.; Mooley, K.P.; Frail, D.A. The GMRT 150 MHz all-sky radio survey. First alternative data release TGSS ADR1. *Astron. Astrophys.* **2017**, *598*, A78. [CrossRef]
107. Gregory, P.C.; Condon, J.J. The 87GB catalog of radio sources. *Astrophys. J. Suppl. Ser.* **1991**, *75*, 1011–1291. [CrossRef]
108. Gordon, Y.A.; Boyce, M.M.; O'Dea, C.P.; Rudnick, L.; Andernach, H.; Vantyghem, A.N.; Baum, S.A.; Bui, J.P.; Dionyssiou, M. A catalog of very large array sky survey epoch 1 quick look components, sources, and host identifications. *Res. Notes AAS* **2020**, *4*, 175. [CrossRef]
109. Chambers, K.C.; Magnier, E.A.; Metcalfe, N.; Flewelling, H.A.; Huber, M.E.; Waters, C.Z.; Denneau, L.; Draper, P.W.; Farrow, D.; Finkbeiner, D.P.; et al. The Pan-STARRS1 Surveys. *arXiv* **2016**, arXiv:1612.05560.
110. Collaboration, G.; Brown, A.G.A.; Vallenari, A.; Prusti, T.; de Bruijne, J.H.J.; Babusiaux, C.; Bailer-Jones, C.A.L.; Biermann, M.; Evans, D.W. ; Eyer, L.; et al. Gaia Data Release 2: Summary of the contents and survey properties. *Astron. Astrophys.* **2018**, *616*, A1. [CrossRef]
111. Lasker, B.M.; Lattanzi, M.G.; McLean, B.J.; Bucciarelli, B.; Drimmel, R.; Garcia, J.; Greene, G.; Guglielmetti, F.; Hanley, C.; Hawkins, G.; et al. The Second-Generation Guide Star Catalog: Description and Properties. *Astron. J.* **2008**, *136*, 735. [CrossRef]
112. Acciari, V.A.; Ansoldi, S.; Antonelli, L.A.; Engels, A.A.; Baack, D.; Babić, A.; Banerjee, B.; De Almeida, U.B.; Barrio, J.A.; González, J.B.; et al. Broadband characterisation of the very intense TeV flares of the blazar 1ES 1959+ 650 in 2016. *Astron. Astrophys.* **2020**, *638*, A14.
113. Yershov, V. Serendipitous UV source catalogues for 10 years of XMM and 5 years of Swift. *Astrophys. Space Sci.* **2014**, *354*, 97–101. [CrossRef]
114. Morrissey, P.; Conrow, T.; Barlow, T.A.; Small, T.; Seibert, M.; Wyder, T.K.; Budavári, T.; Arnouts, S.; Friedman, P.G.; Forster, K.; et al. The calibration and data products of GALEX. *Astrophys. J. Suppl. Ser.* **2007**, *173*, 682. [CrossRef]

115. Page, M.; Brindle, C.; Talavera, A.; Still, M.; Rosen, S.; Yershov, V.; Ziaeepour, H.; Mason, K.; Cropper, M.; Breeveld, A.; et al. The XMM—Newton serendipitous ultraviolet source survey catalogue. *Mon. Not. R. Astron. Soc.* **2012**, *426*, 903–926. [CrossRef]
116. Middei, R.; Giommi, P.; Perri, M.; Turriziani, S.; Sahakyan, N.; Chang, Y.; Leto, C.; Verrecchia, F. The first hard X-ray spectral catalogue of Blazars observed by NuSTAR. *Mon. Not. R. Astron. Soc.* **2022**, *514*, 3179–3190. [CrossRef]
117. Giommi, P.; Brandt, C.; de Almeida, U.B.; Pollock, A.; Arneodo, F.; Chang, Y.; Civitarese, O.; De Angelis, M.; D'Elia, V.; Vera, J.D.R.; et al. Open Universe for Blazars: A new generation of astronomical products based on 14 years of Swift-XRT data. *Astron. Astrophys.* **2019**, *631*, A116. [CrossRef]
118. Evans, P.; Page, K.; Osborne, J.; Beardmore, A.; Willingale, R.; Burrows, D.; Kennea, J.; Perri, M.; Capalbi, M.; Tagliaferri, G.; et al. 2SXPS: An improved and expanded swift X-Ray telescope point-source catalog. *Astrophys. J. Suppl. Ser.* **2020**, *247*, 54. [CrossRef]
119. Giommi, P. Multi-frequency, multi-messenger astrophysics with Swift. The case of blazars. *J. High Energy Astrophys.* **2015**, *7*, 173–179. [CrossRef]
120. Webb, N.A.; Coriat, M.; Traulsen, I.; Ballet, J.; Motch, C.; Carrera, F.J.; Koliopanos, F.; Authier, J.; de La Calle, I.; Ceballos, M.T.; et al. The XMM-Newton serendipitous survey-IX. The fourth XMM-Newton serendipitous source catalogue. *Astron. Astrophys.* **2020**, *641*, A136. [CrossRef]
121. Saxton, R.; Read, A.; Esquej, P.; Freyberg, M.; Altieri, B.; Bermejo, D. The first XMM-Newton slew survey catalogue: XMMSL1. *Astron. Astrophys.* **2008**, *480*, 611–622. [CrossRef]
122. Oh, K.; Koss, M.; Markwardt, C.B.; Schawinski, K.; Baumgartner, W.H.; Barthelmy, S.D.; Cenko, S.B.; Gehrels, N.; Mushotzky, R.; Petulante, A.; et al. The 105-month Swift-BAT all-sky hard X-ray survey. *Astrophys. J. Suppl. Ser.* **2018**, *235*, 4. [CrossRef]
123. Chang, Y.L.; Arsioli, B.; Giommi, P.; Padovani, P.; Brandt, C. The 3HSP catalogue of extreme and high-synchrotron peaked blazars. *Astron. Astrophys.* **2019**, *632*, A77. [CrossRef]
124. Aleksić, J. et al. [MAGIC Collaboration]. The major upgrade of the MAGIC telescopes, Part I: The hardware improvements and the commissioning of the system. *Astropart. Phys.* **2016**, *72*, 61–75. [CrossRef]
125. Daniel, M.; Badran, H.; Bond, I.; Boyle, P.; Bradbury, S.; Buckley, J.; Carter-Lewis, D.; Catanese, M.; Celik, O.; Cogan, P.; et al. Spectrum of very high energy gamma-rays from the blazar 1ES 1959+ 650 during flaring activity in 2002. *Astrophys. J.* **2005**, *621*, 181. [CrossRef]
126. Acciari, M.C.V.; Ansoldi, S.; Antonelli, L.; Arbet Engels, A.; Babić, A.; Banerjee, B.; Barres de Almeida, U.; Barrio, J.; Becerra González, J.; Bednarek, W.; et al. An intermittent extreme BL Lac: MWL study of 1ES 2344+ 514 in an enhanced state. *Mon. Not. R. Astron. Soc.* **2020**, *496*, 3912–3928. [CrossRef]
127. Singh, K.K.; Bisschoff, B.; van Soelen, B.; Tolamatti, A.; Marais, J.P.; Meintjes, P.J. Long-term multiwavelength view of the blazar 1ES 1218+304. *Mon. Not. R. Astron. Soc.* **2019**, *489*, 5076–5086. [CrossRef]
128. Rodrigues, X.; Paliya, V.S.; Garrappa, S.; Omeliukh, A.; Franckowiak, A.; Winter, W. Leptohadronic multi-messenger modeling of 324 gamma-ray blazars. *Astron. Astrophys.* **2024**, *681*, A119. [CrossRef]
129. Wani, K.; Gaur, H.; Patil, M. X-Ray Studies of Blazar 1ES 1959+ 650 Using Swift and XMM-Newton Satellite. *Astrophys. J.* **2023**, *951*, 94. [CrossRef]
130. Krawczynski, H.; Hughes, S.B.; Horan, D.; Aharonian, F.; Aller, M.F.; Aller, H.; Boltwood, P.; Buckley, J.; Coppi, P.; Fossati, G.; et al. Multiwavelength Observations of Strong Flares from the TeV Blazar 1ES 1959+650. *Astrophys. J.* **2004**, *601*, 151. [CrossRef]
131. Sahakyan, N. Lepto-hadronic γ-Ray and Neutrino Emission from the Jet of TXS 0506+056. *Astrophys. J.* **2018**, *866*, 109. [CrossRef]
132. Aguilar-Ruiz, E.; Galván-Gámez, A.; Fraija, N. Testing a Lepto-Hadronic Two-Zone Model with Extreme High-Synchrotron Peaked BL Lacs and Track-like High-Energy Neutrinos. *Galaxies* **2023**, *11*, 117. [CrossRef]
133. Aguilar-Ruiz, E.; Fraija, N.; Galván-Gámez, A. High-energy neutrino fluxes from hard-TeV BL Lacs. *J. High Energy Astrophys.* **2023**, *38*, 1–11. [CrossRef]
134. Sasse, R.; Costa, R., Jr.; Pereira, L.A.S.; dos Anjos, R.C. Blazars Jets and Prospects for TeV-PeV Neutrinos and Gamma Rays Through Cosmic-Ray Interactions. *Braz. J. Phys.* **2025**, *55*, 60. [CrossRef]